Microseismic Bulletin Relationships From Four Years of Monitoring Using Permanent SADAR Arrays

K.D. Hutchenson, P. Nyffenegger, C. Yelton, D. Quigley, and E. Grant, Geospace Technologies

ABSTRACT

A sparse network of four volumetric phased SADAR arrays were installed at Carbon Management Canada's (CMC) Newell County Field Research Station (FRS) southeast of Calgary, Alberta, in the Fall of 2021. Since installation, the network field systems composed of the SADAR arrays, data acquisition, and recording functions have operated at ~99% availability, and that data have been continually processed at an off-site center. The result is a four-year passive monitoring record of the microseismic response at the FRS to CO_2 injection. The curated microseismic bulletin allows a statistical and spatial analysis at a very local level. We report a number of standard seismicity catalog measurements including seismicity rate, b-values, event-array distances, and magnitudes of completeness (Mc), from the extended duration testing and evaluation effort.

INTRODUCTION

Geospace Technologies installed four (4) permanent SADAR compact volumetric phased arrays configured as a sparse network at the Carbon Management Canada (CMC) Field Research Station (FRS) in 2021 for passive microseismic monitoring. The CMC FRS is a proving ground for evaluating measurement, monitoring, and verification (MMV) technologies for geologic carbon storage (GCS) (Lawton *et al.*, 2019; Macquet *et al.*, 2019, 2022). The FRS site hosts other seismic monitoring technologies including a network of three-component surface geophones, a downhole multi-component geophone array, and several surface and borehole DAS runs. Over this four-year reporting period, the CO_2 injection rates at the FRS are approximately 20 tons/year or less into the Basal Belly River Sandstone (BBRS, z~300m). The Newell County region is largely aseismic: a search of the Natural Resources Canada database found no events occurring since the beginning of 2000 within 100 km of Brooks.

Traditional approaches for seismic MMV use networks of surface sensors and downhole sensor strings (*e.g.* Eaton, 2018; Maxwell, 2014). Surface sensors are susceptible to signal-to-noise (SNR) issues from the industrial operations and existing wells for downhole arrays can be scarce. Together these methods are potentially insufficient for satisfying monitoring requirements for large scale GCS. In comparison, sparse networks of SADAR arrays permanently installed in shallow boreholes (9-19 m) offer a durable, proven, and effective alternative. The volumetric phased array designs with individual sensor element acquisition enable techniques for forming simultaneous arbitrary beams. The sparse network thus produces superior data at a lower cost and reduces total risk.

Four years of continuous passive monitoring at the FRS has resulted in a continuous bulletin of events that may reflect the seismic expression related to the amount of CO_2 injected into the BBRS reservoir. The spatial distribution, magnitude frequency distribution (MFD), systems performance, and active source survey capabilities have previously been presented in Grant *et al.* (2025), Hutchenson *et al.* (2025a, 2025b), Nyffenegger *et al.* (2025a, 2025b, 2023, 2022), and Zhang *et al.* (2023b). The continuous bulletin allows investigation of seismogenic processes at full scale, yet over a small highly instrumented volume, in a low stress and mostly aseismic environment, and with highly controlled and measured geological injection operations. In this report, we update the spatial distribution of seismicity, and in addition, report seismicity rate, a refined MFD, and magnitude of completeness (Mc).

METHODS AND RESULTS

SADAR array and sparse network design and installation were previously presented in Nyffenegger *et al.* (2022, 2023a), Zhang *et al.* (2023b), and Hutchenson *et al.* (2023, 2025a). All field systems have been operating at a 99% availability, with system downtime attributable primarily to long duration power outages at the FRS. The SADAR volumetric arrays are connected to single channel 24-bit digitizers running at 2000 samples per second. The system contains a total of 231 vertical geophone channels generating approximately 4 terabytes of SEG-D files per month.

The passive seismic data processing pipeline for the signals collected at the FRS has been operating since late 2021 in an offsite data center. The processing, event detection, and location procedures used for building the bulletin are defined and discussed in Zhang *et al.* (2022), Zhang *et al.* (2023a, b, c), and Hutchenson *et al.* (2023). Analyst curation follows automated processing, together requiring 40 hours for each month of records to produce a refined bulletin with industrial events flagged**.** The bulletin contains hypocenter origin times and locations along with their uncertainty ellipses, and source moment magnitude Mw.

Figure 1 shows the distribution of events both spatially and as a function of depth, the injection well, and the sparse network of SADAR stations. Colors represent the origin time with blue as the older events and red the most recent; symbol size represents Mw. These 1423 events represent the bulletin subset with the best locations, determined using P-

phases with good SNR observed at all four SADAR arrays. Events are clustered around the injection well.

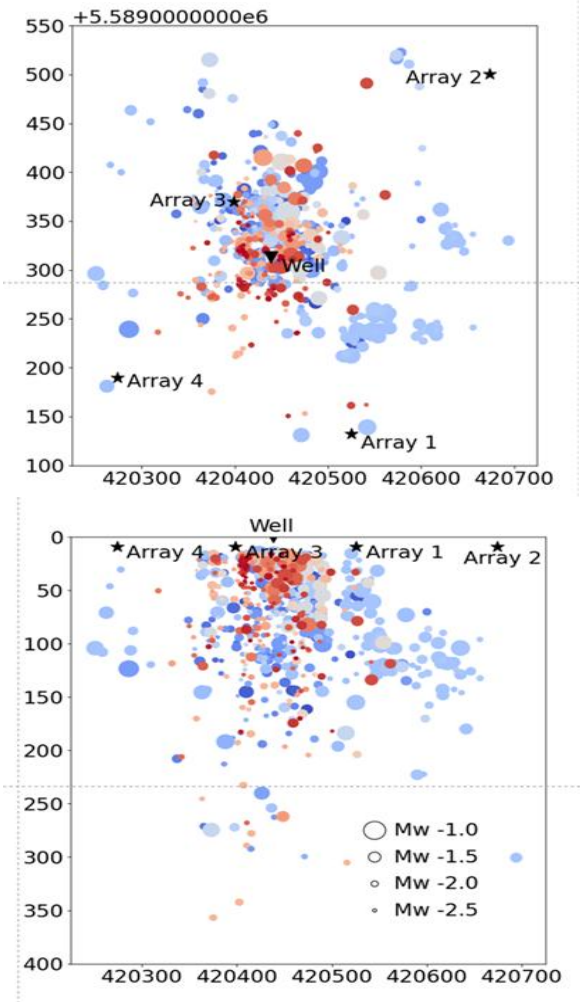

Figure 1. Seismic distribution from 4 years of monitoring. Top is the spatial view with the SADAR array positions shown. The bottom image is a vertical slice.

Once the refined cumulative bulletin is updated, summary statistics are determined, and spatial and time relationships are examined. Traditionally, seismic bulletins play a significant role in the assessment of seismic risk mitigation and earthquake hazards (Mignan and Woessner, 2012). Seismicity rates, referring to the frequency of microseismic events greater than a magnitude cut-off occurring within a defined region or volume, are determined for a discrete time interval, and then as a rolling average to produce a time-series. Seismicity rate observations in mostly aseismic areas with low-pressure fluid injection operations over short and long periods of time are not well represented in the literature.

The seismicity rates for the four years shown in Figure 2 includes all located events from the catalog computed as a rolling average of 4 weeks, offset at (1) week intervals, over the course of the 4-year period (blue line in Figure 2). Complementing the seismic rate is the CO_2 injection rate with the same rolling interval (red).

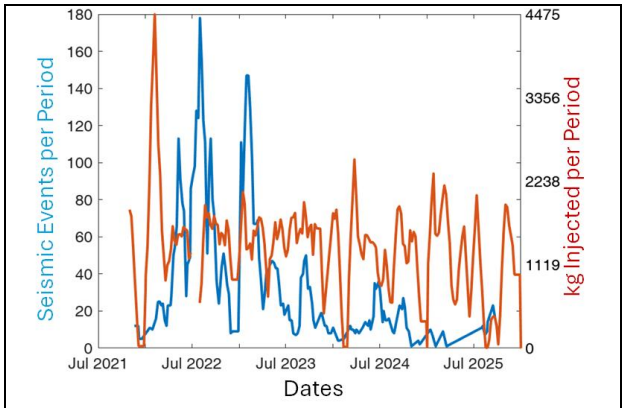

Figure 2. Rolling seismic activity rate and CO_2 injection volumes for four years of data.

Figure 2 suggests relatively constant injection volumes over the four-year period with higher seismicity rates during the early part of the four-year monitoring period beginning in 2022 and ending in the middle of 2023, with a dramatic reduction in seismicity for the latter half of the four-year period.

A reduction of events in later months is not correlated with injected volumes shown in Figure 2. The higher seismicity rates ending prior to July 2023 may be related to the elevated injection volumes in early 2022 (Moein *et al.*, 2025 Verdon *et al.*, 2024; McGarr, 2014). However, consistent injection levels in the latter half of the 4 years correlated with lower seismicity.

Magnitude distribution is a fundamental earthquake scaling relationship. Moment magnitudes are calculated for the FRS bulletin events using the displacement spectra following Brune (1970, 1971) and Shearer (2019) as specified in Zhang *et al.* (2023b). For the events at the FRS, the spectra are best fit using unusually small stress drops as low as 10 Pa and no larger than 10 kPa. The MFD for a population of earthquakes from a limited area and single stress regime is calculated from the magnitude distribution histogram and usually well described using the Gutenberg-Richter (GR) relationship (*e.g.* Shearer, 2019; Eaton, 2018; Grechka and Heigl, 2017; Scholz, 1990):

$$\log(N \geq M) = a - bM$$

where a is the relative activity rate and b defines the slope of the frequency of occurrence fall off with increasing magnitudes. The magnitude frequency characteristics of

microseismicity generally follow the same power law relationship as observed for tectonic earthquake catalogs (Maxwell, 2014). This type of power law distribution, typical of fractal sets, arises from the self-similarity of earthquakes and is genetically related to self-similar sizes of faults and joints (Scholz, 1990). However, other MFD models may also be more appropriate. There are a variety of methods for fitting power law parameters and selection of MFD model in the literature (*e.g.*, Li and Avouac, 2026).

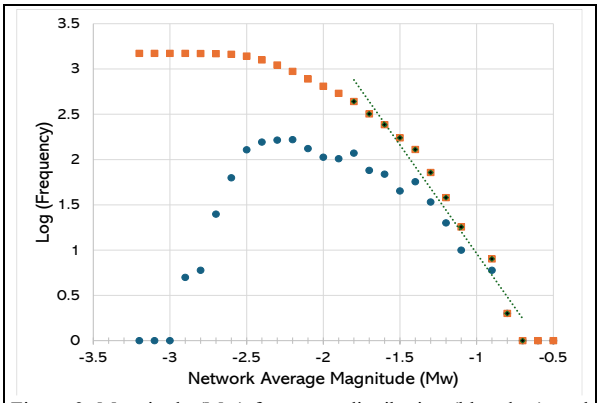

Figure 3. Magnitude (Mw) frequency distribution (blue dots), and cumulative magnitude frequency distribution (N≥M) (orange squares) for events located within the network. The small blue triangles indicate the data used to determine the Gutenberg-Richter relationship (dotted line).

The MFD result for four years of monitoring is provided in Figure 3. The overall histogram does not conform to expectations for a standard GR model. GR relationship parameters determined using a standard linear fit over the range Mw=[-1.8, -0.7] are b =-2.4 with a=-1.4 with an R^2=0.96. For tectonic earthquake catalogs, the value for b typically falls within a range between 0.8-1.2 (*e.g.*, Frohlich and Davis, 1993), except for cases of earthquake swarms and event clusters where it is sometimes relatively elevated (Scholz, 1990), such as reported with reservoir fracturing engineering (Vogelaar *et al.*, 2013; Eaton *et al.*, 2014), and volcanic activity (Jacobs and McNutt, 2010). For example, Vogelaar *et al.* (2013) report b-values as high as 5 and 6.

Fitting the Gutenberg-Richter relationship parameters over the range Mw=[-2.5, -1.4] results in b = 0.94 with a = 0.88 and R^2=0.97, more in line with cases reported in Eaton and Maghsoudi (2015). For comparison, a strictly empirical quadratic fit over the range Mw=[-2.5, -0.7] has the form:

$$\log(N \geq M) = -1M^2 - 4.9M - 2.8$$

with R^2=0.994. For the FRS, the cluster of events around the injection well is expected but may not necessarily originate with critically stressed faults. Other MFD models exist in the literature, for example the tapered Gutenberg-Richter relation as summarized in Li and Avouac (2026) that may better fit these observations. In addition, biases may exist in the bulletin and in determining the model parameters (*e.g.*, Geffers *et al.*, 2022).

El-Isa and Eaton (2013) discuss a number of causes related to b-value variation. Chief among these for this area, is an increase or decrease in effective stress and variations attributable to tectonic characteristics. Note this area is aseismic with low crustal stress levels as derived from determining stress-drop in conjunction with Mw. However, domains in the MFD curve illustrated with multiple b-values may suggest changing conditions (Jacobs and McNutt, 2010).

The magnitude of completeness Mc can be defined as the magnitude above which the catalog is considered complete with no missing events (Eaton, 2018). A variety of methods for determining Mc exist in the literature such as Weimer and Wyss (2000), Mingnan and Woessner (2012), and Wang *et al.* (2025). The magnitude distribution histogram shown in Figure 3 suggests a Mc of approximately -2.5 Mw because of the dramatic change in population for less energetic events as executed in Eaton and Maghsoudi (2015). This assessment of Mc is strictly judgmental because of the non-standard magnitude distribution histogram.

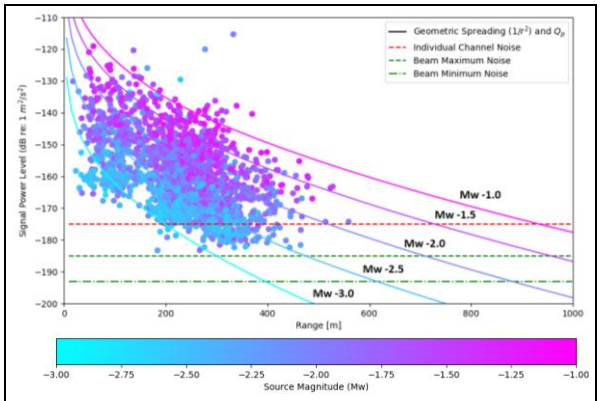

Figure 4. Received signal power versus source-receiver range for 545 well located events color coded by Mw. Events with depth greater than 25 m, within 275 m of the injection well, and with arrival times clearly seen on all arrays are included.

Examining the received signal power level on each array as a function of distance (Figure 4) provides a different view of the minimum magnitude limit for locatable events used in conjunction with Figure 3 for estimating Mc (after Eaton, 2018). The detection range limits and therefore completeness estimates vary with the signal propagation loss. Propagation loss depends on event-array distance due to spherical spreading and frequency dependent on attenuation of the signals. Figure 3 is constructed using 545 events having the number of time-defining phases ndef=4 (with depths greater than 25 m, and within 275 m of the

injection well. For the FRS network, ndef=4 indicates that obvious P-wave arrivals were detected on all four SADAR arrays. One point is plotted for each array for each event, for a total of 2180 points, and the modeled received signal level curves as a function of magnitude (solid lines) are also plotted, including estimated propagation loss. In addition, noise estimates are plotted for the single channel noise average level (red dashed line) and then applying both the estimated beam minimum (green dashed) and maximum noise suppression (green dash-dot) from measured array gains.

Combined, the located event populations, the magnitude frequency distribution from Figure 3, and information derived from Figure 4 support an Mc estimate around -2.5 Mw within the monitored volume near the injection well. These estimates are also supported by performance models presented in Grant *et al.* (2025), and validated in part by the SADAR sparse network bulletin.

CONCLUSIONS

Four years of persistent passive microseismic monitoring of the CMC FRS delivered using the permanent SADAR sparse network proves the SADAR network and processing systems reliability. The data center semi-automated operations routinely perform the signal processing, detection, association, and location functions while also tracking system state of health and data quality. The curated seismic bulletin is evidence of the consistency of the SADAR sparse network for microseismic monitoring at the FRS.

The bulletin allows additional statistical and spatial analysis at a very local level contributing to the overall extended duration testing and evaluation of the sparse network. The standard analysis of seismicity rate, magnitude distribution b-values, and Mc result in measurements or features that are either continuously monitored or periodically assessed, used as indicators of the geophysical state of the underground assets. Observed seismicity rates are only loosely correlated with the volume of injected CO_2. This result is expected because of the low injected volumes and rates.

Additional work is required to determine the MFD model that best describes the observations, and therefore the extent of self-similar scaling behavior in this low stress drop, low pressure environment. The results of the piece-wise fits of the empirical b-value curve fit suggest the microseismicity at the Newell County FRS may be better described by a non-Gutenberg-Richter relationship. Alternatively, the MFD may be indicative of a mixture of multiple distributions.

For the FRS, the magnitude distribution histogram suggests a Mc=-2.5 Mw. In addition, the received signal power vs. distance point cloud fits nicely between $-3 \leq Mw \leq -1$ with a cutoff of 400 m. Measured noise levels and array gains and modeled received signal power levels of -2.5 Mw and -3 Mw support a Mc=-2.5 Mw assessment.

The long-term performance of the SADAR sparse network demonstrates not only technical reliability but also a commercially viable pathway for operators seeking cost-effective, regulatory-aligned monitoring solutions for CCUS and other subsurface operations. The automated processing, including a near real-time variant, low operational overhead, and the ability to extract actionable indicators of geophysical state, provides operators with a scalable, low-risk, long life monitoring platform. With the phase 1 engineering of the SADAR sparse network processing pipeline complete, system development has shifted to deriving information from the cumulative bulletin useful to operators. As we transition into the next phase, our focus is on delivering operator-ready dashboards, near real-time alerts, and decision-support tools that translate the cumulative bulletin information into operational value. For example, the seismicity rate, moment release as a function of time, and cumulative (net) seismic moment are tracked using techniques like “control charts” available to operators with daily updates. Other examples include cluster analysis based spatial statistics of the noise and seismicity, sequential analysis, and hazard analysis. These capabilities position SADAR as a strategic partner for operators looking to enhance subsurface assurance while managing cost and regulatory expectations.

ACKNOWLEDGEMENTS

Geospace Technologies acknowledges Carbon Management Canada for access to the Newell County Field Research Station and operational data. The Field Research Station is funded by the Joint Industry Project. The authors also acknowledge financial support from Emission Reduction Alberta (ERA) through the Advanced Multi-Physics Sparse Monitoring (AMPS) project and the Government of Alberta through the Technology Innovation Emissions Reduction (TIER) Fund.